1. Redouane MIMOUNI, 2. Azzedine HAMID, 3. Aicha FLITTI, 4. Abderrahim MOKHEFI,
5. Fatima Zohra MEDJAOUI, 6. Mohamed RIZOUGA

OPEN ACCESS

DOI: 10.15199/48.2025.06.27

Magnetothermal behaviour analysis of a planar microtrans-former

Analiza zachowania magnetotermicznego płaskiego mikrotransformatora

Abstract: *This paper explores in depth the magnetothermal behaviour of a micro-transformer, an essential component in low-power energy conversion systems. As part of this study, we carried out precise dimensioning, aimed at defining the various geometric and electrical parameters essential to the optimal design of the micro-transformer. Stacked planar transformers represent a significant technological advance in the field of electromagnetic devices. This work focuses on the analysis of the magnetothermal behaviour of these transformers, combining the magnetic and thermal effects associated with their operation. The study examines magnetic performance, taking into account losses in the laminated magnetic cores, as well as Joule effect losses in the windings. Particular attention is paid to the internal heating of the micro-transformer due to loss dissipation, which can alter its magnetic properties and reduce its overall efficiency. In parallel, the study included a detailed thermodynamic analysis to understand the temperature distribution throughout the device. This analysis took into account heat transfer processes by conduction through the solid materials, as well as by convection at the interfaces with the external environment. These phenomena were studied in steady state, i.e. considering stable thermal conditions after a certain operating time. The results obtained provide valuable information for optimizing the thermal design of the micro--transformer, in order to ensure its long-term reliability and performance. The methodology is based on multi-physics modelling and numerical simulation to predict thermal and magnetic behaviour under various operating conditions. The results show that the choice of materials, stack geometry and heat dissipation techniques play a key role in the design of more efficient and durable transformers. This work opens the way to optimizations in the fields of power electronics and high-frequency applications.*

Streszczenie: *W artykule tym szczegółowo zbadano zachowanie magnetotermiczne mikrotransformatora, istotnego elementu w systemach konwersji energii o niskiej mocy. W ramach tego badania przeprowadziliśmy precyzyjne wymiarowanie, mające na celu zdefiniowanie różnych parametrów geometrycznych i elektrycznych niezbędnych do optymalnego zaprojektowania mikrotransformatora. Transformatory planarne ułożone jeden na drugim stanowią znaczący postęp technologiczny w dziedzinie urządzeń elektromagnetycznych. Niniejsza praca koncentruje się na analizie zachowania magnetotermicznego tych transformatorów, łącząc efekty magnetyczne i termiczne związane z ich działaniem. Badanie bada wydajność magnetyczną, biorąc pod uwagę straty w laminowanych rdzeniach magnetycznych, a także straty efektu Joule'a w uzwojeniach. Szczególną uwagę zwrócono na wewnętrzne nagrzewanie się mikrotransformatora z powodu rozpraszania strat, co może zmienić jego właściwości magnetyczne i zmniejszyć jego ogólną wydajność. Równolegle badanie obejmowało szczegółową analizę termodynamiczną w celu zrozumienia rozkładu temperatury w całym urządzeniu. Analiza ta uwzględniała procesy wymiany ciepła poprzez przewodzenie przez materiały stałe, a także poprzez konwekcję na stykach ze środowiskiem zewnętrznym. Zjawiska te badano w stanie ustalonym, tj. biorąc pod uwagę stabilne warunki termiczne po pewnym czasie pracy. Uzyskane wyniki dostarczają cennych informacji do optymalizacji projektu termicznego mikrotransformatora, w celu zapewnienia jego długoterminowej niezawodności i wydajności. Metodologia opiera się na modelowaniu wielofizycznym i symulacji numerycznej w celu przewidywania zachowania termicznego i magnetycznego w różnych warunkach pracy. Wyniki pokazują, że wybór materiałów, geometrii stosu i technik rozpraszania ciepła odgrywają kluczową rolę w projektowaniu bardziej wydajnych i trwałych transformatorów. Praca ta otwiera drogę do optymalizacji w dziedzinach elektroniki mocy i zastosowań wysokoczęstotliwościowych.*

Keywords: Flyback converter, micro-transformer, passive components, magneto thermal
Słowa kluczowe: Przetwornica flyback, mikrotransformator, elementy pasywne, magnetotermiczne

Introduction

The use of discrete components has significant limitations, particularly in terms of size. Their size and large number take up a lot of space on circuits, making them difficult to integrate into compact systems. In addition, the hundreds of soldering points required to assemble them increase the risk of failure, affecting the overall reliability of electronic devices. To meet these challenges, research is focusing on the miniaturization of components, an area that has led to the development of integrated passive components [1] [2] [3] [4]. This concept involves manufacturing components by integrating them directly as groups on a common substrate, rather than individually. This approach reduces space requirements, improves reliability by reducing the number of solder points, and optimises the performance of electronic circuits [5] [6] [7]. With the proliferation of portable devices such as computers, mobile phones, cameras and flat screens, the demand for miniaturised voltage transformers has increased considerably [8] [9] [10] [11]. These devices meet growing demands for compactness, light weight and energy efficiency. The micro-transformer, for example, offers reduced dimensions, increased lightness and a high degree of electrical insulation. It is ideal for applications where space and weight are major constraints. In addition, their adaptability to automated manufacturing reduces costs while guaranteeing optimum performance. Among micro--transformer configurations, two types stand out: stacked transformers and interleaved transformers [12] [13] [14]. Stacked micro-transformers, the subject of our work, superimpose two coils on several metal layers, allowing high magnetic coupling and optimum use of the surface area. However, this configuration generates parasitic capacitances, which can limit their performance, particularly at high frequencies.

As part of this work, a study was carried out on a stacked micro-transformer (see Figure 1). It consists of two superimposed circular coils, each placed on a separate substrate. Each substrate incorporates an insulating layer for electrical separation and a magnetic layer to ensure efficient coupling. Copper was chosen as the winding material for the primary and secondary coils, because of its advantages. The choice of magnetic material is crucial for the integration of passive components, as it helps to increase the value of the inductance, confine the magnetic field lines, maximise energy storage and significantly reduce the number of turns. To meet these requirements, we selected a ferrite ($NiFe_2O_4$) because of its high relative permeability and high electrical resistivity. For the insulating material, we chose Kapton, renowned for its excellent dielectric properties, perfectly suited to this type of application. The physical phenomenon studied is described by Maxwell's equations, governing the electromagnetic aspects, closely coupled to the heat equation, representing the thermal behavior [15] [16] [17]. The following assumptions are made: the buoyancy of the air in the vertical direction is negligible, and the primary and secondary microcoils are considered as internal heat sources.

The system of partial differential equations, together with boundary conditions, is solved using the finite element method implemented in Comsol 5.6 software. This micro-transformer is intended for insertion in a flyback DC-DC micro-converter, in the low-power, low-voltage range. The constraints associated with this type of integration lie in the development of a suitable method for sizing the integrated micro-transformer, with minimum losses at high frequencies.

The choice of structure for our micro-converter is fairly straightforward, since it's not a question here of trying to find an innovative structure and studying its advantages and disadvantages, but of using a basic structure so that it can be integrated without too much difficulty.

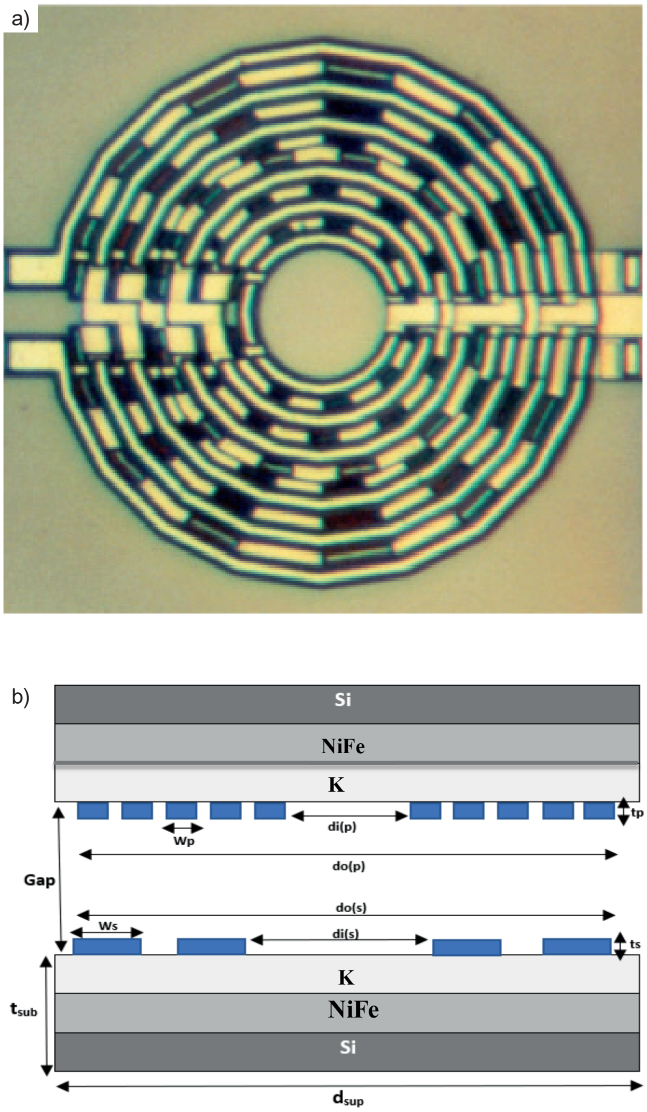

Fig. 1: (a) Example of a stacked planar micro-transformer, (b) longitudinal section of the stacked micro-transformer

Flyback micro-converter presentation

The Flyback micro-converter was chosen because it consists of a reduced number of components, a single wound component – the micro-transformer – and a single switch (see Figure 2). In addition, it is frequently used for low-power applications (< 100W). We have opted for the specifications from which we define the specifications of the micro-converter which constitutes the starting point for the dimensioning of the micro-transformer: Input voltage Ve=12 V, Output voltage Vs=5V, Output power Ps=5W, Operating frequency f= 100 MHz

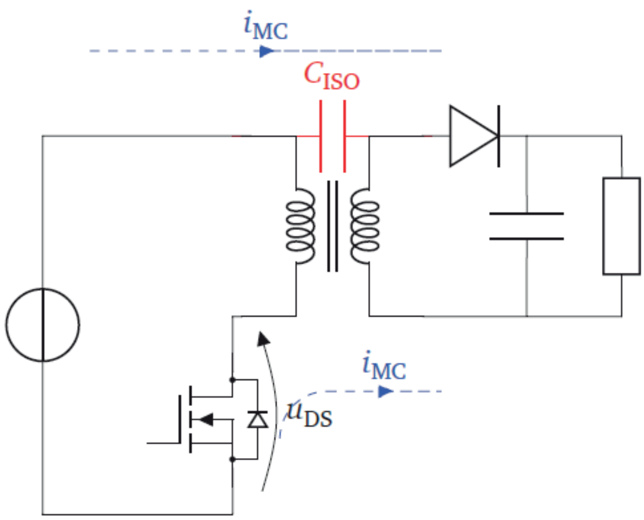

Fig. 2. Electrical diagram of the selected flyback converter

Design of the micro-coils making up the micro-transformer

By taking into account certain electrical and magnetic characteristics of the micro-transformer, the volume of the magnetic core and the surface on which the micro-transformer's electrical circuit will be placed can be evaluated. The dimensions of the magnetic core will then be evaluated, in line with the specifications of the micro-converter in terms of magnetic energy storage and material losses.

For example, consider the primary microcoils (the same will apply to the secondary) (see Figure 3).

The coil is in the form of a circular spiral, also known as an Archimedean coil. It consists of two juxtaposed curves (C1) and (C2), of n turns, in the horizontal plane Oxy. θ = 0 corresponds to the starting point of the two spirals, their width is wi. θ = 2nπ, corresponds to the end of the two spirals, their width is noted w (wi for a variable width coil), (see Figure 4).

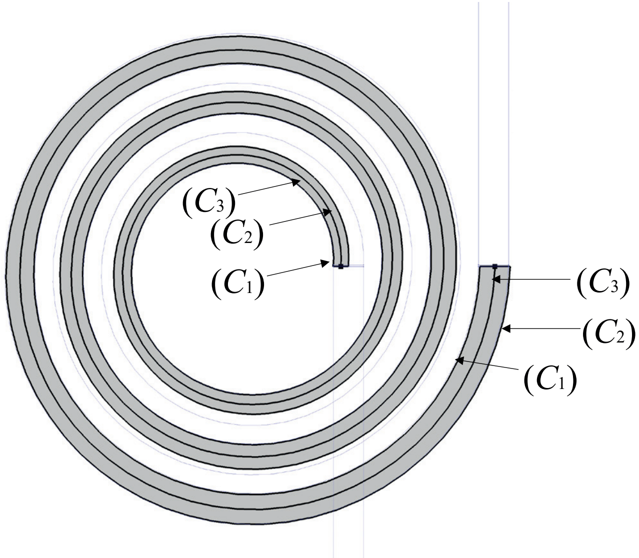

Fig. 3: Example of primary (or secondary) coil design with variable conductor width

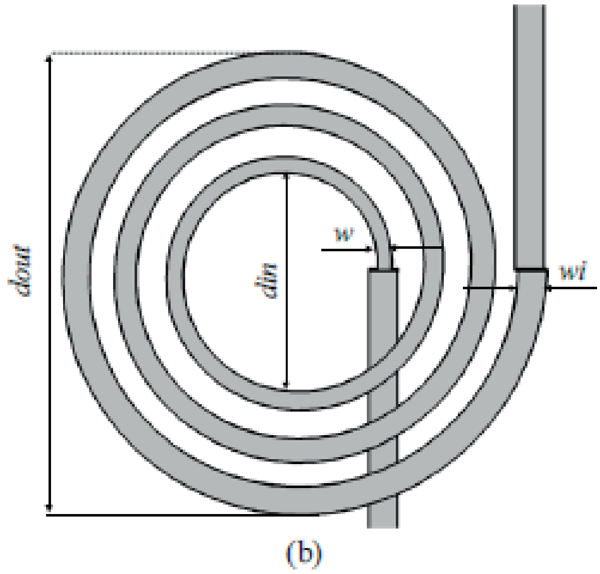

Fig. 4. The sizes used to build the reels

The equations governing these two spirals are shown below.

(1) $$(C_1): r_1(\theta) = a_1\theta + b_1,\ (C_2):\ r_2(\theta) = a_2\theta + b_2$$

With a1, a2, b1, b2 coefficients given by the formulae given below: Equations from (2) to (6).

(2) $$a_1(w) = \frac{2n\left[d_{out} - d_{in} - 2w\right]}{4n\pi(2n-1)}$$

(3) $$b_1(w) = \frac{d_{in} - \pi a_1}{2}$$

(4) $$a_1(w) = \frac{2n\left[d_{out} - d_{in} - 2w\right]}{4n\pi(2n-1)}$$

(5) $$a_2(w) = a_1$$

(6) $$b_2(w) = w + b_1$$

The total lengths of the fixed- and variable-width coils are calculated from the median curve (C3), (see Figure 4). The equation governing this curve is of the following form:

(7) $$(C_3): r_3(\theta) = a_3\theta + b_3$$

with:

(8) $$a_3(w) = a_1$$

(9) $$b_3(w) = \frac{w}{2} + b_1$$

For a coil with a fixed width (w = wi), the length is expressed by the following relationship:

(10) $$L_f = 2n\pi\left[a_3(w)n\pi + b_3(w)\right]$$

The cross-section varies as a function of θ and is given by the following formula:

(11) $$S = t \times w(\theta)$$

On the other hand, in the case of a variable width coil (wi ≠ w), the total length of the variable coil is expressed by the following relationship:

(12) $$L_v = 2n\pi\left[a_3(w)n\pi + b_3(w)\right]$$

In this case, the conductor cross-section is not constant. The cross-section of the spiral coil decreases as a function of the curvilinear abscissa. The average cross-section can be expressed as a function of the inner diameter:

(13) $$\overline{S} = t_{eq}\left[n\pi\left(a_2(w) - a_1(w)\right) + \left(b_2(w) - b_1(w)\right)\right]$$

In fact, varying the width of the coil leads to a reduction in its cross-sectional area, resulting in an increase in the electrical current density. Therefore, to keep the electrical behavior of the two fixed and variable width micro-coils almost identical, their electrical resistances must be identical. It is therefore necessary to determine a new thickness teq for the variable-width microcoils:

(14) $$R_{DC}(w_i) = R_{DC}(w) \Rightarrow \frac{L_t(w_i)}{S} = \frac{L_t(w)}{\overline{S}}$$

The equivalent thickness of the turn can be expressed as a function of the internal diameter of the turn as follows:

(15) $$t_{eq} = \frac{L_t(w) \times t \times w_i}{L_t(w_i)\left[n\pi\left(a_2(w) - a_1(w)\right) + \left(b_2(w) - b_1(w)\right)\right]}$$

Sizing the magnetic circuit

The transformation ratio m is one of the main electrical parameters of the micro-transformer and is given by:

(16) $$m = \frac{\alpha}{\alpha - 1}\frac{V_{out}}{V_{in}} = 0.417$$

The primary micro-coil inductance Lp is calculated for a maximum current ripple:

$$L_p = \frac{V_{in}^2 \alpha^2}{2.f.P_{out}} \tag{17}$$

The secondary microcoil inductance Ls is taken from equation (18).

$$L_s = m^2 L_p \tag{18}$$

The total stored magnetic energy is therefore:

$$W = \frac{1}{2} L_p i_{in}^2 = \frac{1}{2} L_s i_{out}^2 = 3.125.10^{-9} J \tag{19}$$

The maximum volumetric energy density is equal to:

$$W_{v\max} = \frac{B_{\max}^2}{2.\mu_{NiZn}} = 25.59 J / \mathrm{m}^3 \tag{20}$$

The volume of the core is:

$$V = \frac{W}{W_{v\max}} = 1.22.10^{-10} m^3 \tag{21}$$

Thus, 0.122 mm3 of $NiFe_2O_4$ is required to store 3.125 nJ. The thickness of the core is expressed by the following relationship:

$$e_{NiFe_2O_4} = \frac{V}{d_{out}^2} \tag{22}$$

Below are the geometric parameters of the coils we have chosen, the primary and secondary coils and the substrates.

- Inner diameter d_{in} (μm) =1000
- Outer diameter d_{out} (μm) =10000
- Conductor width w (μm) =600
- Conductor thickness t (μm) =35
- Number of micro-coil turns: n_1=3 et n_2=4
- Length of Kapton substrate L_k (mm) =25.53
- Kapton substrate length $L_{NiFe2O4}$ (μm) =25.53

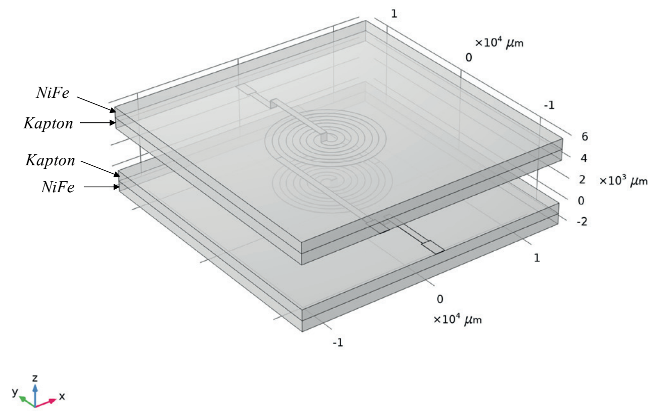

Fig. 6. Micro-transformer with lower and upper substrates

- Kapton substrate thickness w_K (μm) =1000
- Thickness of wNiFe2O4 substrate (μm) =1000

Physical model of the planar micro-transformer

The stacked-structure micro-transformer that is the subject of our study consists of two coils, the primary and secondary, made of copper and both deposited on two identical substrates at the top and bottom (see Figure 5). The two substrates are made of Kapton, which acts as an insulator, and NiFe2O4, a magnetic material (see Figure 6).

Magneto thermal behavior of the micro-transformer

Governing equations

The electromagnetic phenomenon is governed by Maxwell's equations (see equations 23), the resolution of which will enable us to visualize the magnetic behavior of the planar micro-transformer [12, 13].

$$\nabla \times \vec{H} = \vec{J}\,,\ \nabla \times \vec{A} = \vec{B}\,,\ \vec{E} = -\nabla V - j\omega \vec{A}\,,$$
$$\vec{J} = \sigma \vec{E} + j\omega \vec{D}\,,\ \nabla.\vec{J} = 0\,,\ \vec{B} = \mu_0 \mu_r \vec{H}\,,\ \vec{D} = \varepsilon_0 \varepsilon_r \vec{E} \tag{23}$$

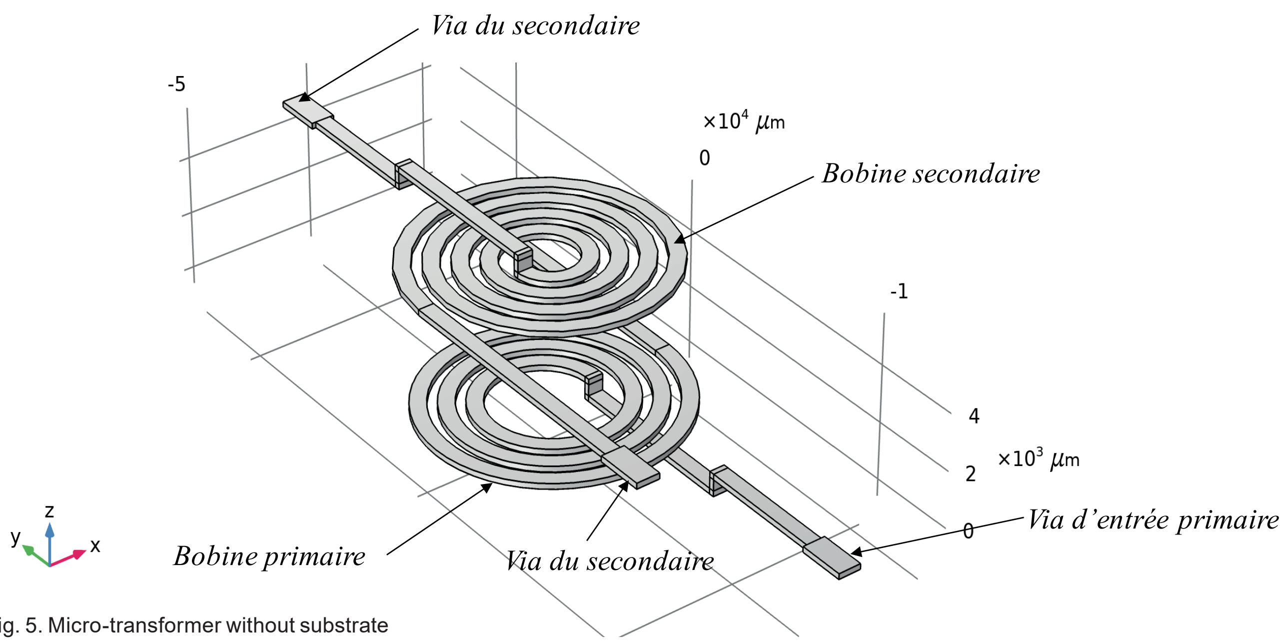

Fig. 5. Micro-transformer without substrate

General simulation conditions

The boundary conditions at the boundaries of the study area, shown in Figure 7, are as follows:

At the primary p and secondary s inlets:

(24) (Primary) : $I = I_p$ et (Secondary) : $I = I_s$, $V_p = V_s = 0$

nd

Other borders:

(25) $$\vec{n}.\vec{A} = 0, \ \vec{n}.\vec{J} = 0$$

Figures 8, 9 and 10 illustrate these conditions.

Solving the mathematical model

To implement the finite element method predefined in the Comsol software, it is essential to introduce a suitable mesh grid to obtain accurate results. To achieve this, we opted for an extremely fine tetrahedral mesh (see Figure 11). This mesh is finer inside the domain and particularly in the immediate vicinity of the two micro-coils (see Figure 12).

Magnetic simulation results and discussion

Electrical current density

Figures 13 and 14 show the current density distribution at the turns of the primary and secondary microcoils. It can be seen that the electrical current density in the primary micro--coil is greater than that in the secondary. As a result, the Joule effect losses are greater in this micro-coil, resulting in a high heat flow and a rise in temperature. The highest electrical current densities occur at the centre of each micro-coil, particularly at the boundaries with a small radius of curvature (see Figure 15 in particular).

The current density distribution was plotted along the horizontal line passing through the primary windings as shown

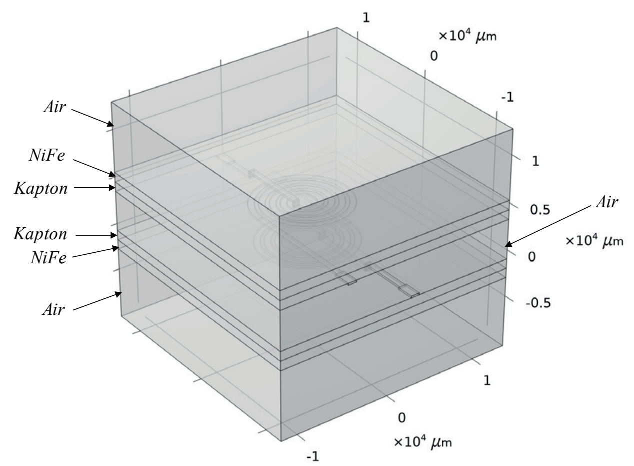

Fig. 7. Study area consisting of the micro-transformer's micro-coils, the substrates and the air

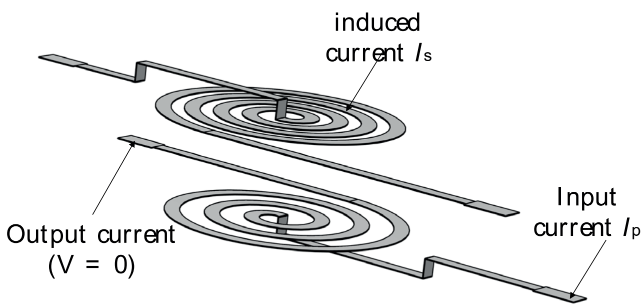

Fig. 8.Initial operating conditions of the planar transformer.

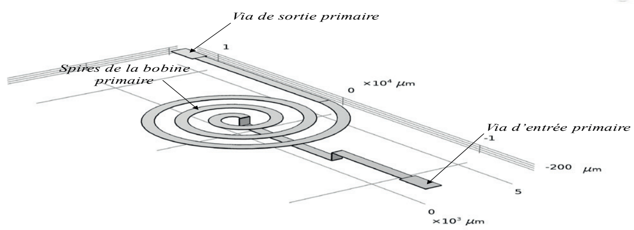

Fig. 9. primary micro-coil

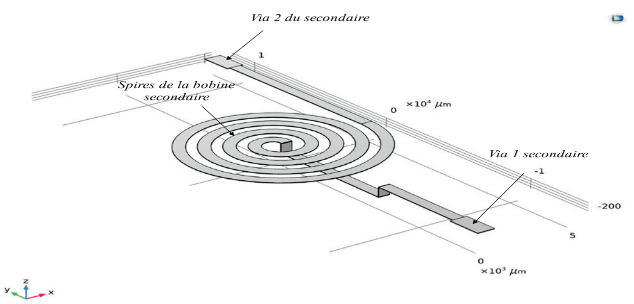

Fig. 10. Secondary microcoils

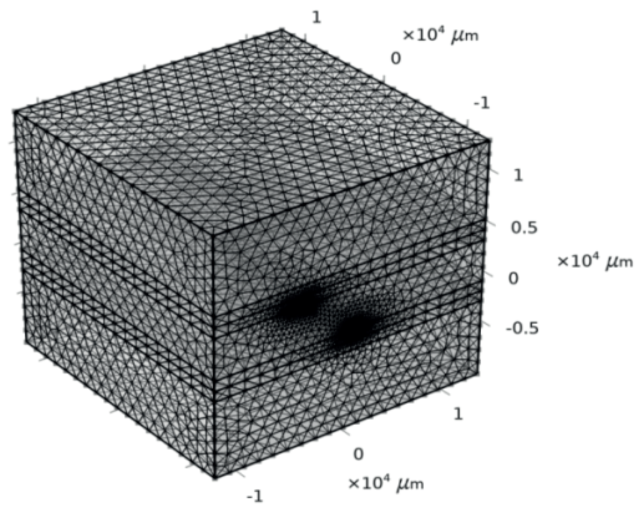

Fig. 11. Meshing of the study area

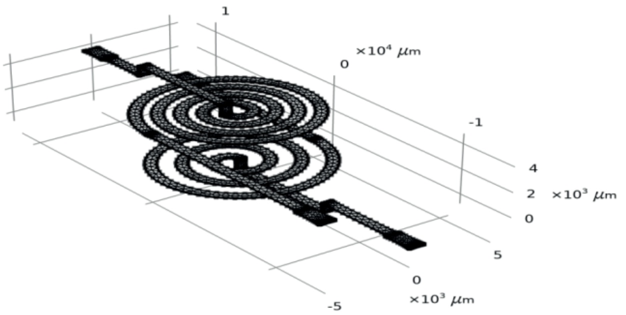

Fig. 12. Meshing of the two micro-coils

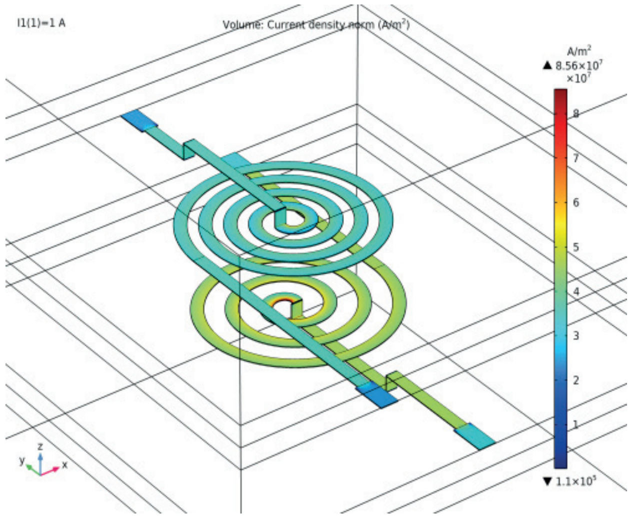

Fig. 13. Current density distribution at the microcoils turns, 3D view

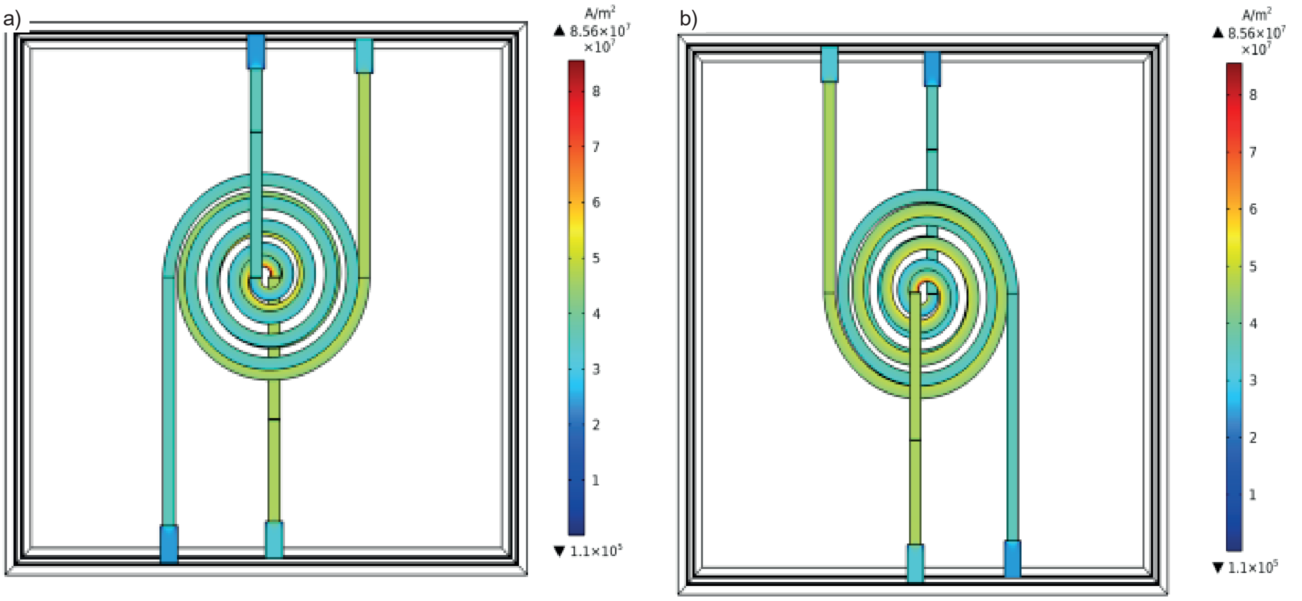

Fig. 14. Distribution of the current density in the turns of the micro-coils: (a) primary and (b) secondary

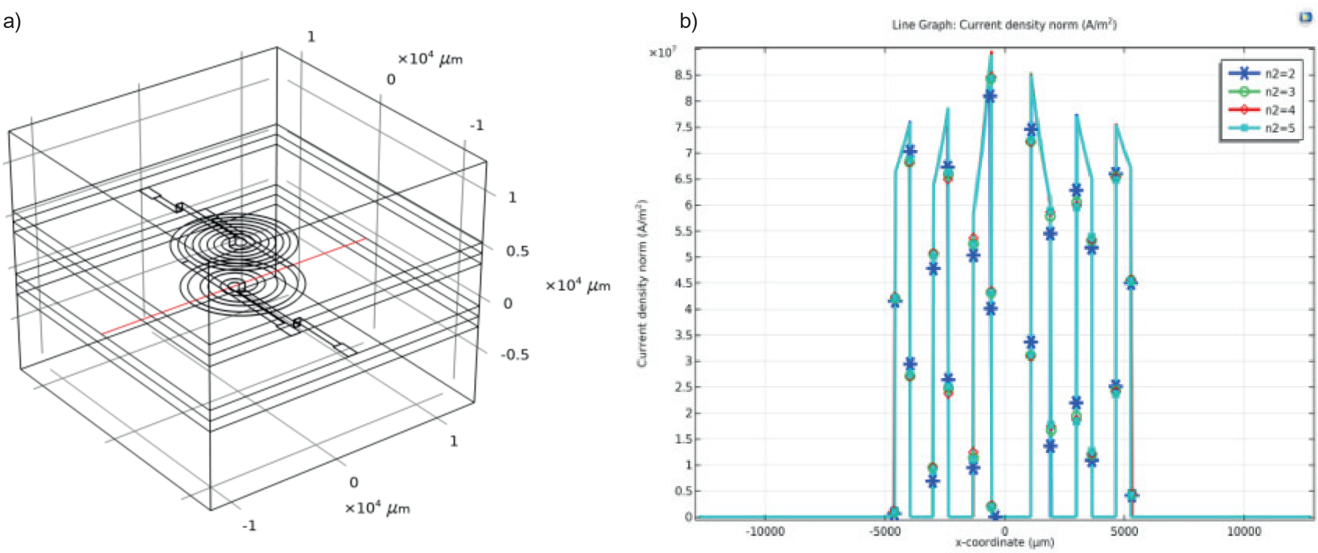

Fig. 15. Distribution of the current density along the horizontal line passing through the primary windings. (a) horizontal line, (b) current density

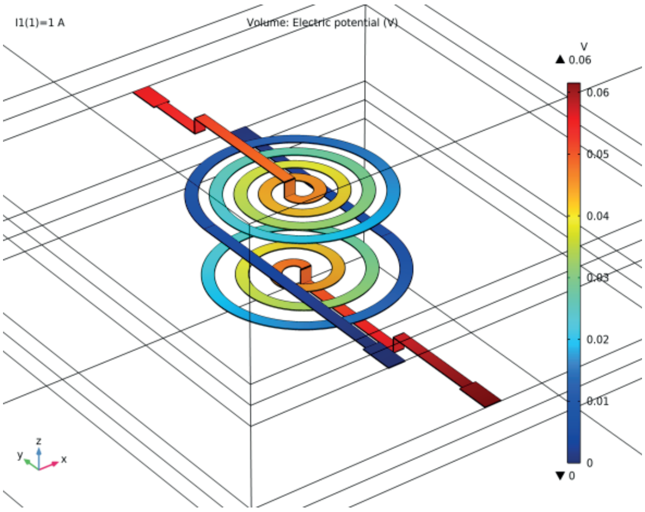

Fig. 16. Distribution of the electrical potential at the level of the turns of the micro-coils, 3D view

in Figure 15. It can be seen that along this line, the current density increases across the turns. In each turn on the left-hand side, the current density increases linearly from the outer circumference (larger radius of curvature) to the inner circumference (smaller radius of curvature).

The current density in the middle turn has a low value compared to the other turns and a higher value at the inner circumference. This is due to the reduced radius of curvature of the inner turns. The behavior is identical for the right-hand turns.

Electrical potential

Figures 16 and 17 show the distribution of the electrical potential at the turns of the micro-coil. It can be seen that the potential is greatest at the input vias of the primary and secondary microcoils.

Figure 18 shows the variation in electrical potential for different values of the number of secondary turns (with n1 fixed at 3). It can be seen that the potential falls slightly at the magnetic substrate and rises sharply in the Kapton layer and in the areas close to the primary turns. Unlike the electric current density, the potential is higher in the secondary. This potential drops in the upper magnetic substrate to become constant in the upper air part with a high value compared to the lower air. As for the influence of the number of turns, the lower the number of turns (n2 = 2), the higher the potential at the secondary and its immediate vicinity.

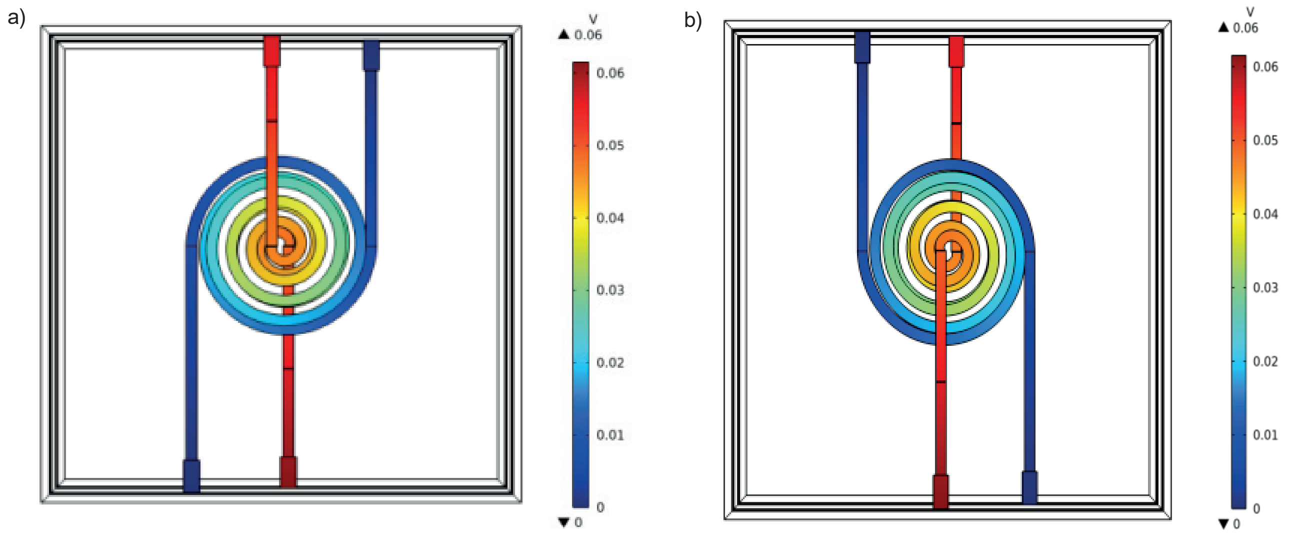

Fig. 17. Distribution of electrical potential at the turns of the micro-coils: (a) primary and (b) secondary

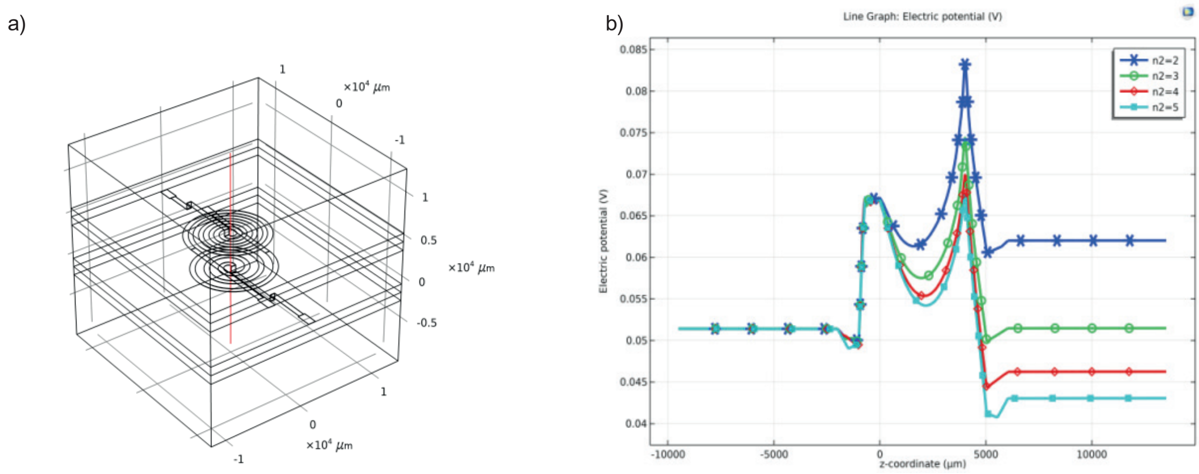

Fig. 18. (a) Vertical line, (b) Distribution of the electric potential along the median vertical line for different numbers of turns.

Magnetic field

Figure 19 shows the distribution of the magnetic field lines and the magnetic field strength at the turns of the micro-transformer. These figures show that the magnetic field is stronger in the inner turns of the two coils, particularly in the vicinity of the areas where the radius of curvature is smallest.

Figure 20 shows the current lines and the magnetic field in vector form. It can be seen that the magnetic field exits the secondary towards the primary in the area outside the transformer.

Figures 21 and 22 show the distribution of the magnetic flux density in the substrate. It can be seen that the magnetic field is strongest at the turns and at the magnetic substrate.

Figures 23 and 24 are vertical sections in which the direction of the magnetic field is clearly visible. In fact, it is directed from the primary towards the secondary in the (internal) gap zone.

Figures 25 to 28 show the distribution of the magnetic field horizontally at different levels. These plans clearly show that the highest magnetic field value is located at the level of the turns and the magnetic substrate.

Micro-transformer thermal behavior

The heat equation allows us to visualize the temperature profile in the two microcoils [15, 16, 17].

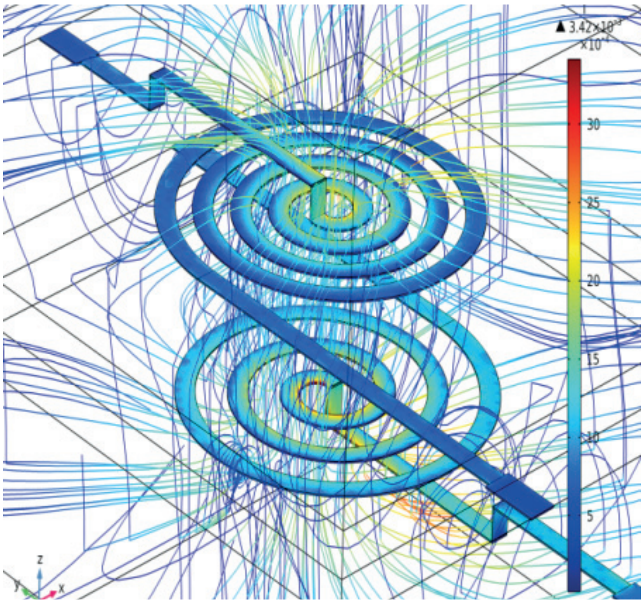

Fig. 19. Distribution of the magnetic field and current lines on the turns of the microcoils (3D view)

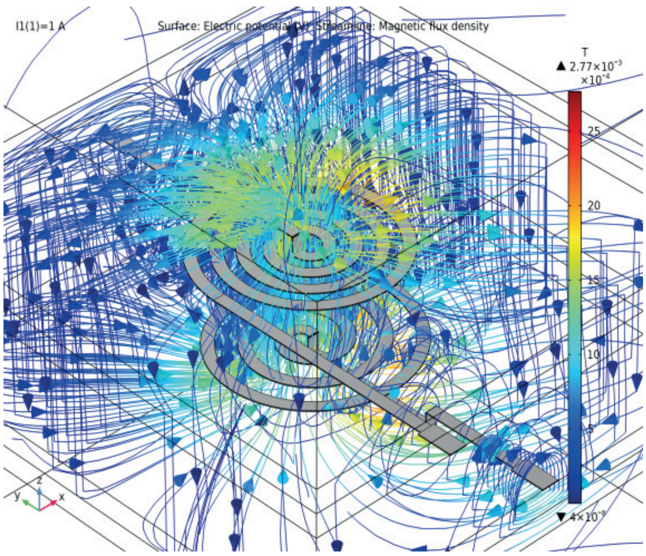

Fig. 20. Distribution of the magnetic field (vectors) and current lines at the level of the turns of the micro-coils (3D view)

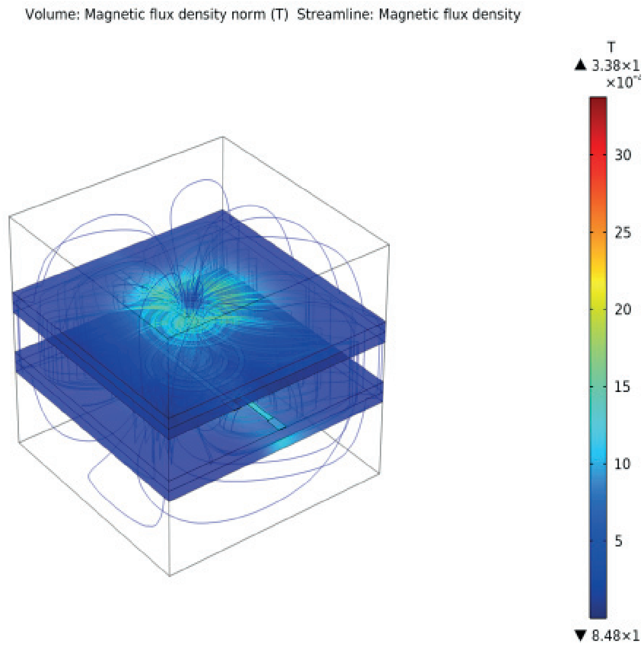

Fig. 21. Distribution of the magnetic field and current lines in the study area (3D view)

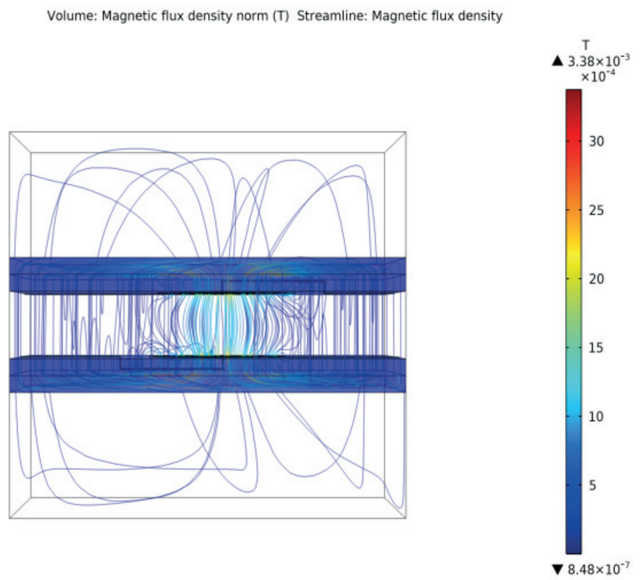

Fig. 22. Distribution of the magnetic field and current lines in the study area (front view)

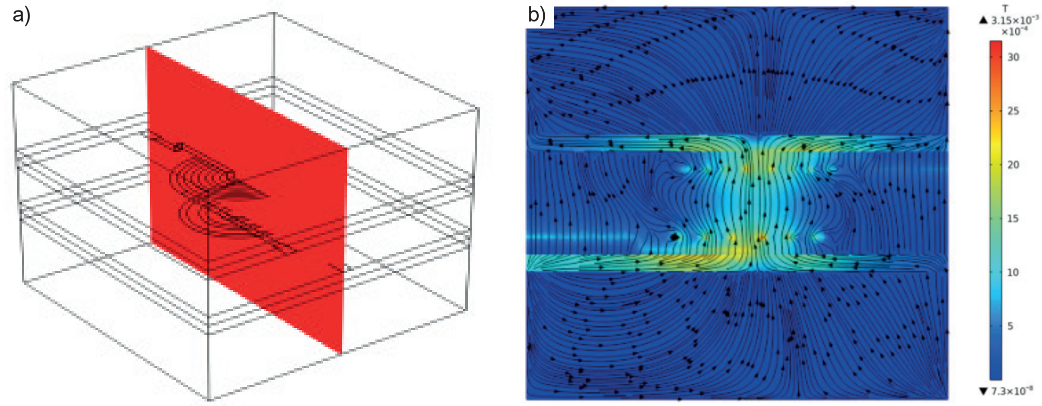

Fig. 23. (a) Vertical plane OYZ, (b) Magnetic field distribution in the micro-transformer along this plane

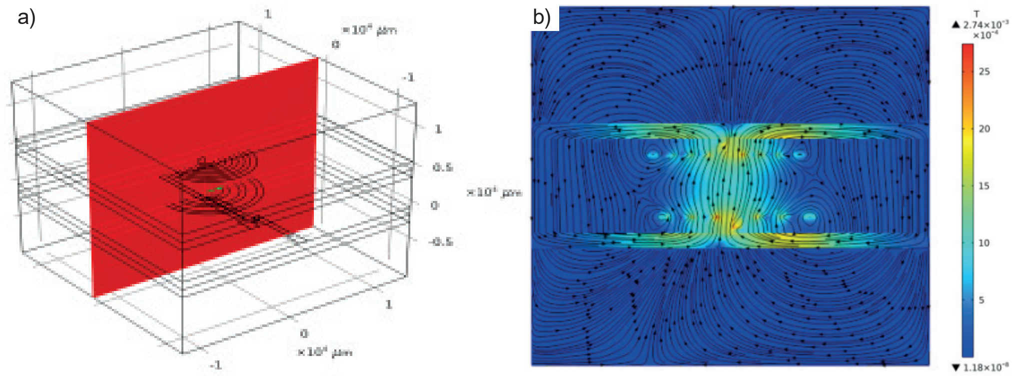

Fig. 24. (a) Vertical plane OXZ, (b) Magnetic field distribution in the micro-transformer along this plane

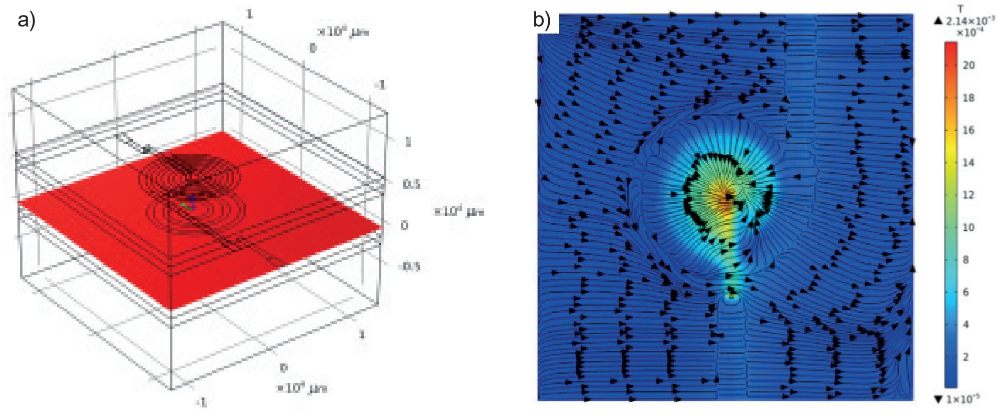

Fig. 25. (a) Horizontal plane OXY in the middle of the Kapton, (b) Distribution of the magnetic field along this plane (in the middle of the Kapton of the primary microcoils)

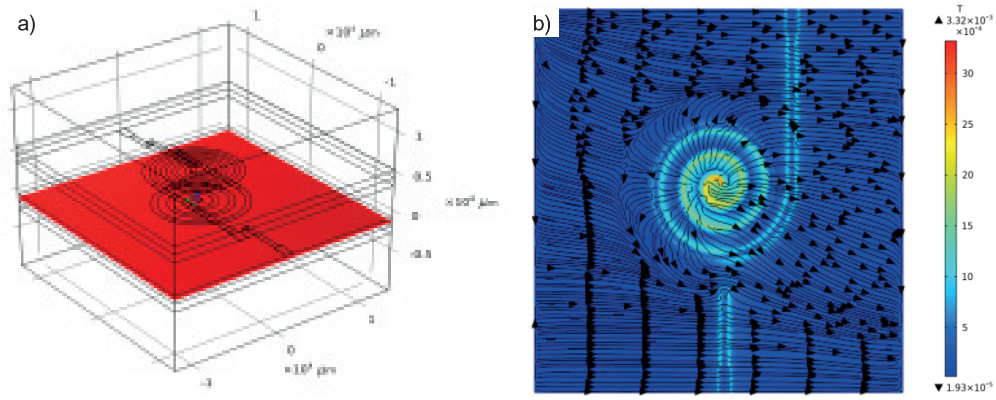

Fig. 26. (a) Horizontal plane OXY at the level of the primary windings, (b) Distribution of the magnetic field in the primary microcoils windings

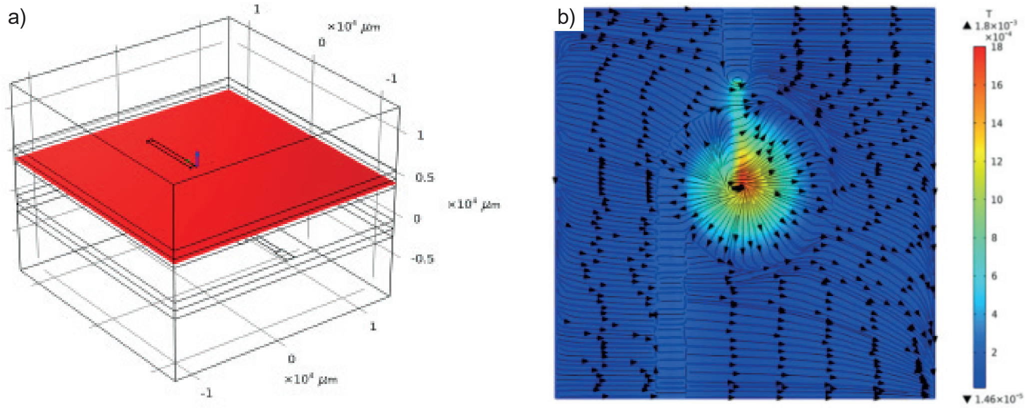

Fig. 27. (a) Horizontal plane OXY at the level of the primary windings, (b) Distribution of the magnetic field along this plane (in the middle of the Kapton of the secondary microcoils)

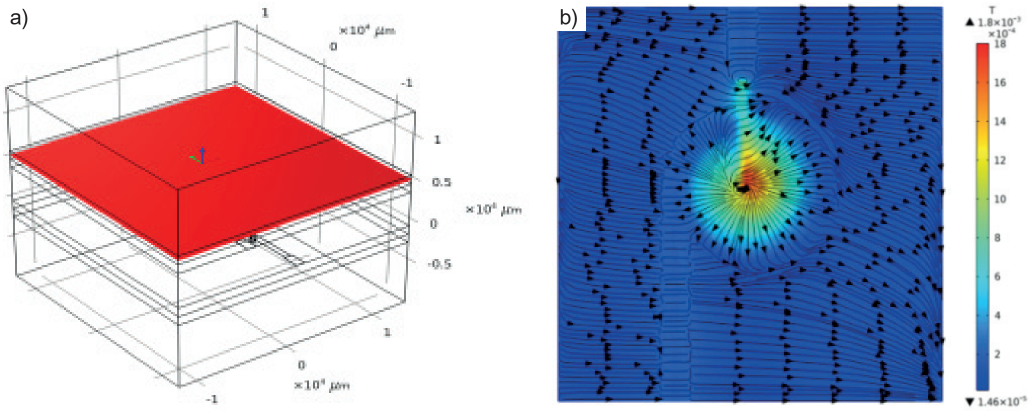

Fig. 28. (a) Horizontal plane OXY in the middle of the secondary NiFe2O4, (b) Distribution of the magnetic field along this plane (in the middle of the secondary NiFe2O4 microcoils)

Governing equations

Equation (29) is used to determine the temperature distribution in a given medium:

(29) $$\rho_i Cp_i\left(\frac{\partial T}{\partial t}\right)=k_i\nabla^2 T+Q$$

$\rho_i Cp_i \partial T/\partial t$: Term used to indicate the storage of heat over time (accumulation);
$\nabla(\lambda_i \nabla T)$: Term used to indicate the propagation method depending on the nature of the material (diffusion);
Q : Source term (internal heat generation).

In a 3D system, equation (29) is written as:

(30) $$\rho_i Cp_i\left(\frac{\partial T}{\partial t}\right)=k_i\left(\frac{\partial^2}{\partial x^2}+\frac{\partial^2}{\partial y^2}+\frac{\partial^2}{\partial z^2}\right)T+Q$$

With $\vec{V}=(u,v,w)$

(31) $$\rho_i Cp_i\left(\frac{\partial T}{\partial t}\right)=k_i\left(\frac{\partial^2}{\partial x^2}+\frac{\partial^2}{\partial y^2}+\frac{\partial^2}{\partial z^2}\right)T+Q$$

(32) $$\rho_i Cp_i\left(\frac{\partial T}{\partial t}+u\frac{\partial T}{\partial x}+v\frac{\partial T}{\partial y}+w\frac{\partial T}{\partial z}\right)$$
$$=k_i\left(\frac{\partial^2 T}{\partial x^2}+\frac{\partial^2 T}{\partial y^2}+\frac{\partial^2 T}{\partial z^2}\right)+Q$$

For negligible convection: The velocity components are zero u = v = w = 0:

(33) $$\rho_i Cp\frac{\partial T}{\partial t}_i=k_i\left(\frac{\partial^2 T}{\partial x^2}+\frac{\partial^2 T}{\partial y^2}+\frac{\partial^2 T}{\partial z^2}\right)+Q$$

And if the case is stationary:

(34) $$k_i\left(\frac{\partial^2 T}{\partial x^2}+\frac{\partial^2 T}{\partial y^2}+\frac{\partial^2 T}{\partial z^2}\right)+Q=0$$

The equation used to calculate the heat is coupled to Maxwell's equations by calculating the current density:

(35) $$\text{Puissance}=R\left\|\vec{i}\right\|^2=S^2R\frac{\left\|\vec{i}\right\|^2}{S^2}=S^2R\left\|\vec{J}\right\|^2$$

The source term Q is given by:

(36) $$Q=\frac{\text{Puissance}}{\text{Vo}}$$

Boundary conditions

The micro-coil is a heat source, and its term is well introduced into equation (34). At time t=0, the temperature of the coil, substrate and air is taken to be the ambient temperature of 20°C. The boundaries of a box of air are provided with a convective flux given by the equation below:

(37) $$-\lambda_{air}\left.\frac{\partial T}{\partial n}\right)_{\text{frontière de l'air}}=h_0(T-T_\infty)$$

λ_{air} : air conductivity [W/m.K],

n : normal direction to the border [m], h_0 : air convection coefficient [W/m^2.°K], T_∞ : Ambient temperature.

Thermal model resolution

The thermal mathematical model is solved by coupling the heat equations and Maxwell's equations, taking into account the terms reflecting the effects of electrical density losses, as described above. The mesh used for this resolution is identical to that used for the magnetic simulation. Consequently, no new mesh is presented in this section.

Results and discussion of micro-transformer thermal behavior

The results of numerical simulations for the thermal component are presented in this section.

Figures 29 and 30 show the temperature profile in the study area. The current flowing in the primary coil is 1A. The maximum temperature is 28.7 °C. This is the hottest part, due to the intensity of the current, which is the main source of heat. For the secondary micro-coil, the temperature reaches 26.6 °C. Thermal convection due to air is not taken into account because the movement of its particles is weak. The following figures show the temperature gradient in the study area. Figures 31 and 32 show the temperature distribution in the primary and secondary windings of the micro-transformer.

In order to better visualize the thermal behavior of the micro-transformer and the various substrates, cross-sections of the study area were made along the OYZ, OXZ planes for different levels in the vertical direction (OXY plane). Figures 33 to 41 show the temperature distribution and the isotherms for different sections of the study area. For ease of reading, the positions of the different planes in the study area are shown to the left of the temperature planes. For the OYZ and OXZ planes passing through the media in the study area (see Figures 33 and 34), the temperature distribution and the isotherms are virtually identical. The temperature is high at and near the primary microcoils and decreases with distance from the primary. On the other hand, the isotherms show closed contours around the primary microcoils. However, in the secondary, the isotherms do not close. This is because the rise in temperature has caused the isotherms to close around the primary coils. It should be noted that the isotherms are open. The OXY plane passes through the middle of the $NiFe_2O_4$ layer, (see figure.35), the isotherms take on an almost circular and concentric shape with a temperature of 28.1°C at its centre.

In the OXY plane passing through the middle of the Kapton layer (see Figure 36). Given the low thermal conductivity of Kapton, the isotherms take the shape of the turns of the microcoils because of the proximity of this layer to the microcoils.

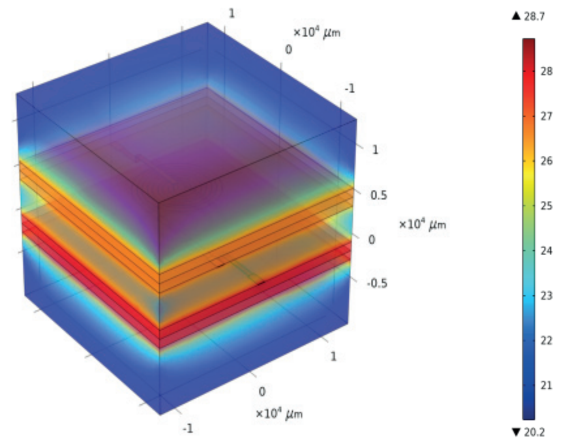

Fig. 29. Temperature distribution in the study area

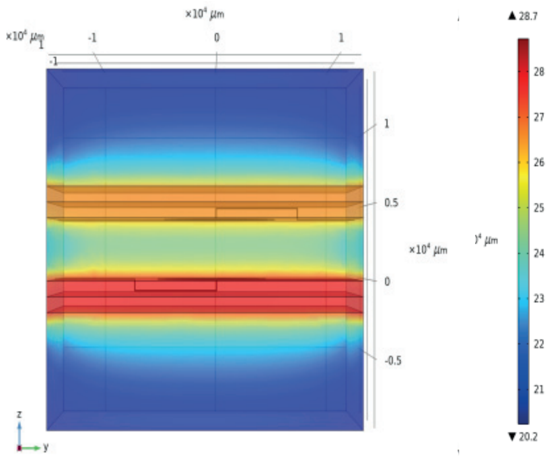

Fig. 30. Temperature distribution in the study area according to the OYZ plane

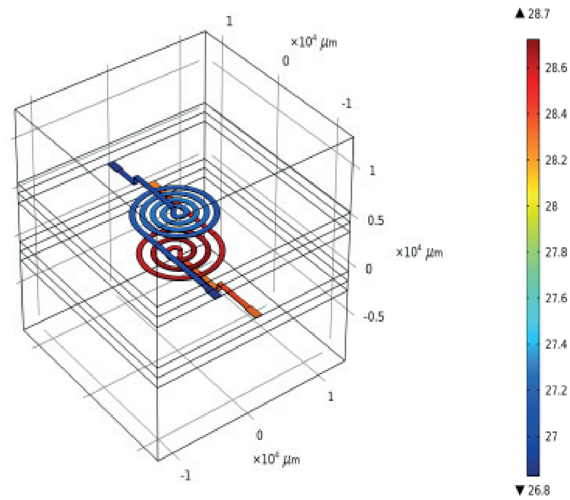

Fig. 31. Temperature distribution across the turns of the micro-transformer

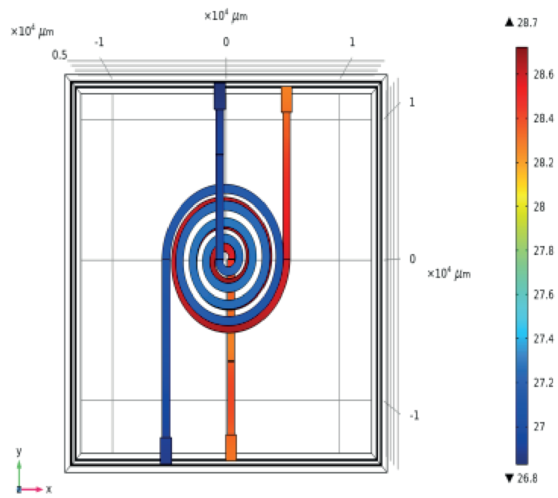

Fig. 32. Temperature distribution across the turns of the micro-transformer (top view)

In the OXY plane passing through the primary turns (see Figure 37), the isotherms are curved and concentrated around the outer turns of the microcoils. These isotherms become almost linear at the vias and the outermost turn, which is due to the higher thermal conductivity of copper compared with Kapton.

At the level of the OXY plane passing through the middle of the gap (see Figure 38), the isotherms become almost square as we move away from this point.

Figures 39 to 41 show the planes passing through the turns of the secondary, the Kapton and the ferrite in the upper part. It can be seen that the behavior is almost identical to that described above, except that the temperature value is lower. The thermal profiles and isotherms are therefore symmetrical. Figure 39 shows the OXY cross-section passing through the air in the upper part. The thermal profiles and isotherms are similar to those found in the space between the primary and secondary microcoils.

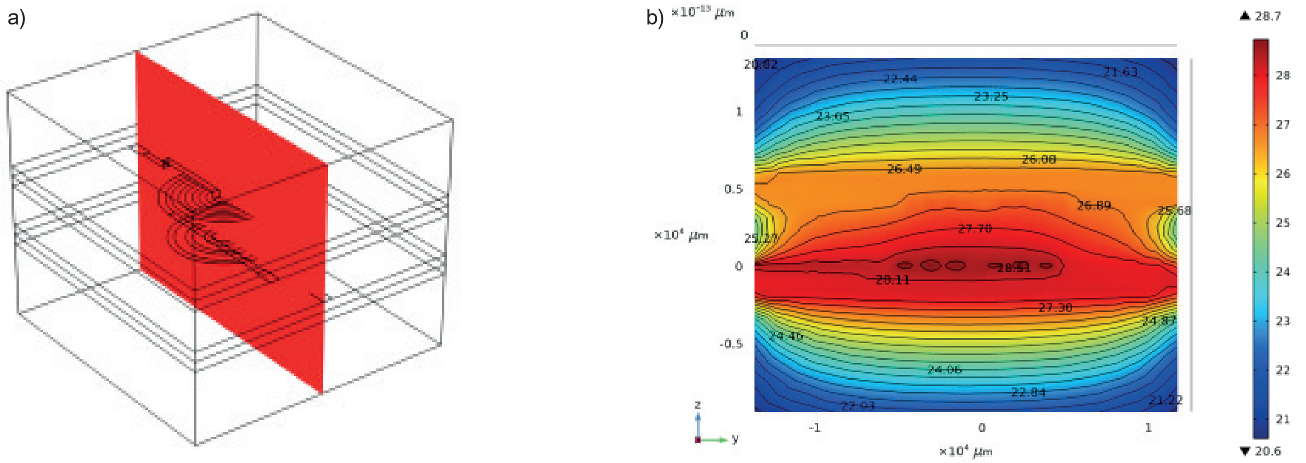

Fig. 33. (a) Vertical plane OYZ, (b) Temperature distribution in the study area and isotherm curve

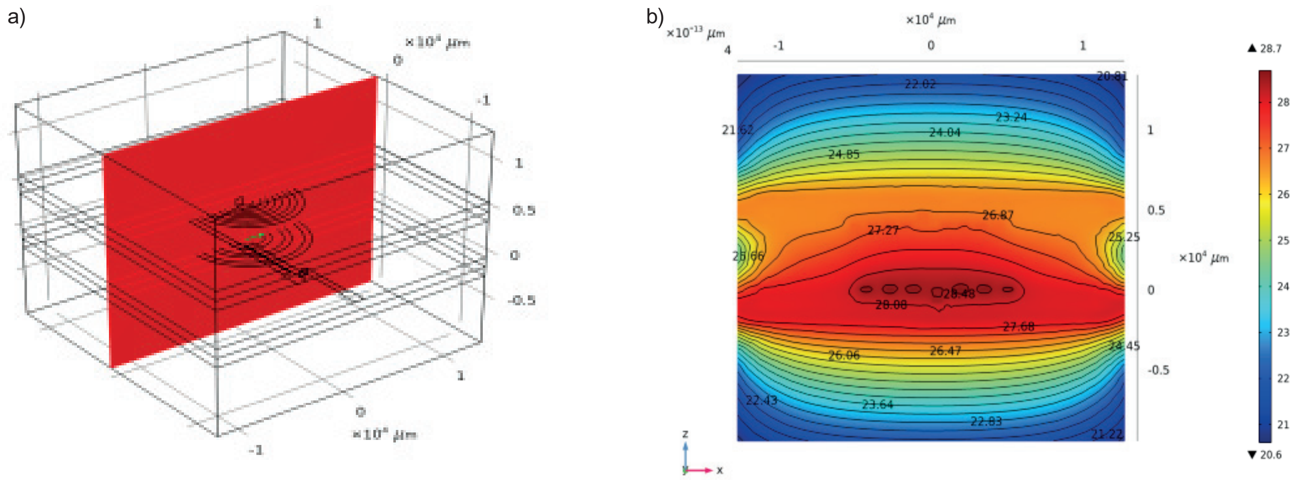

Figure. 34. (a) Vertical plane OXZ, (b) Temperature distribution in the study area and isotherm curves.

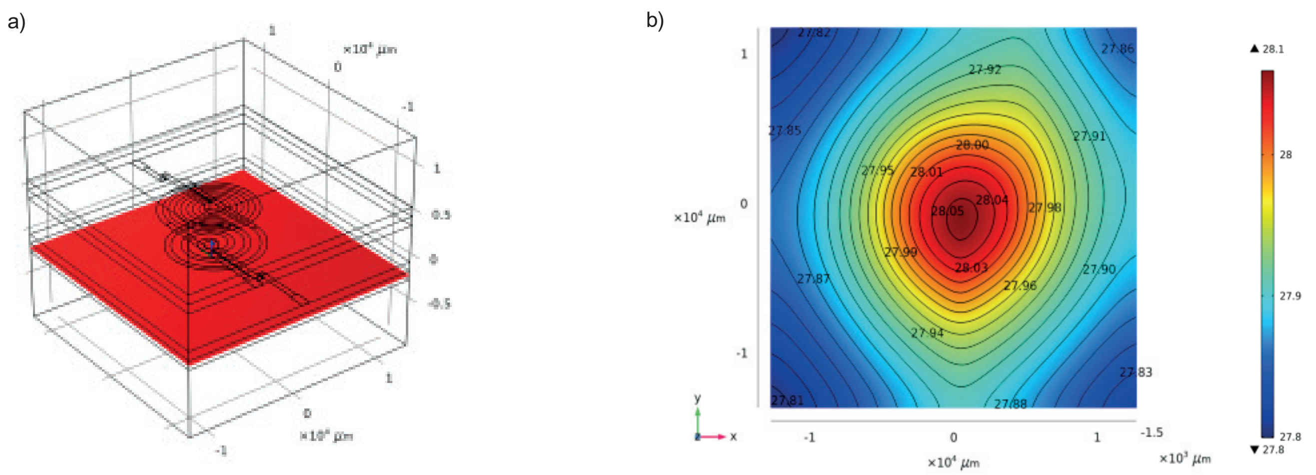

Fig. 35. (a) OXY vertical plane, (b) Temperature distribution in the middle of the NiFe2O4 of the primary micro-coil and the isothermal curve

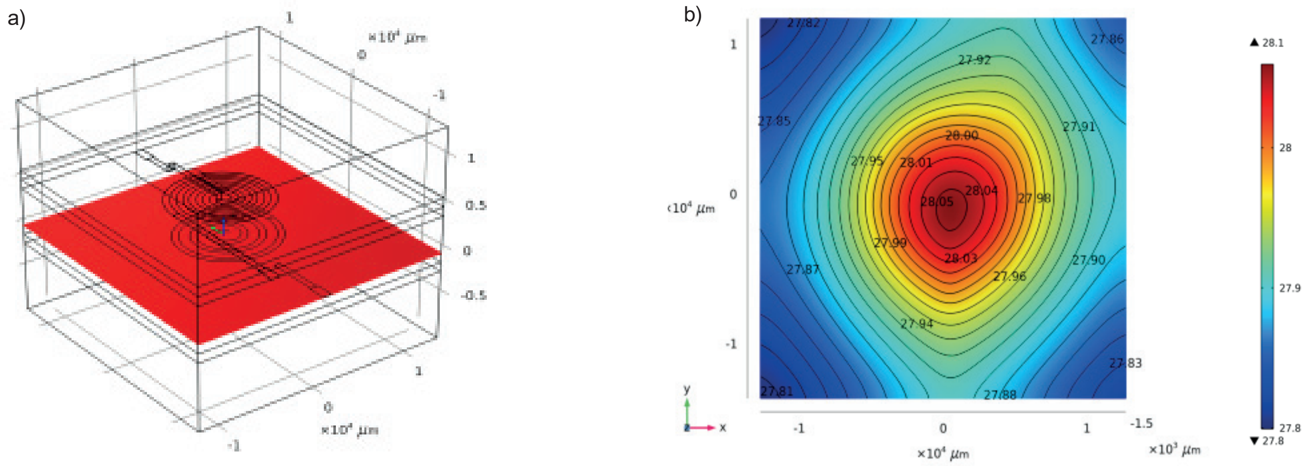

Figure.36. (a) Vertical plane OXY, (b) Temperature distribution in the middle of the Kapton layer of the primary micro-coil and isotherm curve

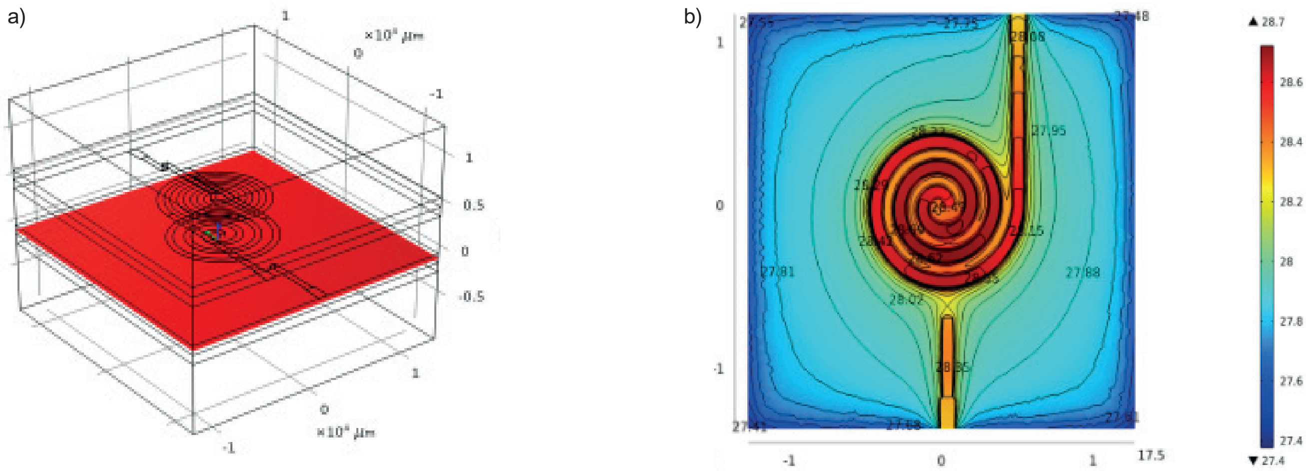

Figure.37. (a) Vertical plane OXY, (b) Temperature distribution at the primary coil turns and isotherm curve

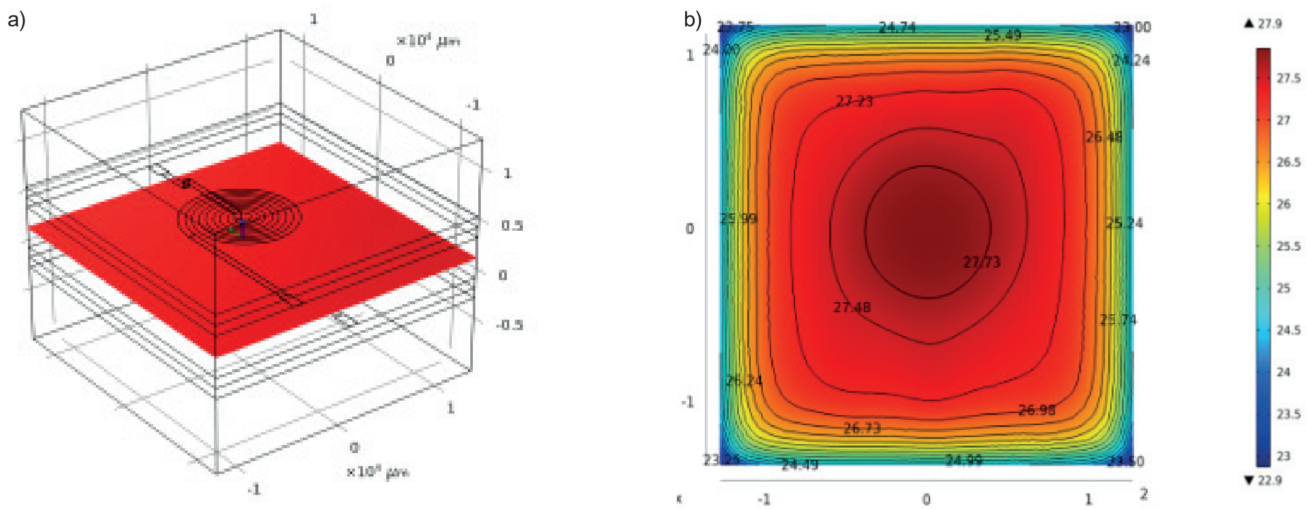

Figure.38. (a) Vertical plane OXY, (b) Temperature distribution in the middle of the space between the microcoils and the isothermal curve

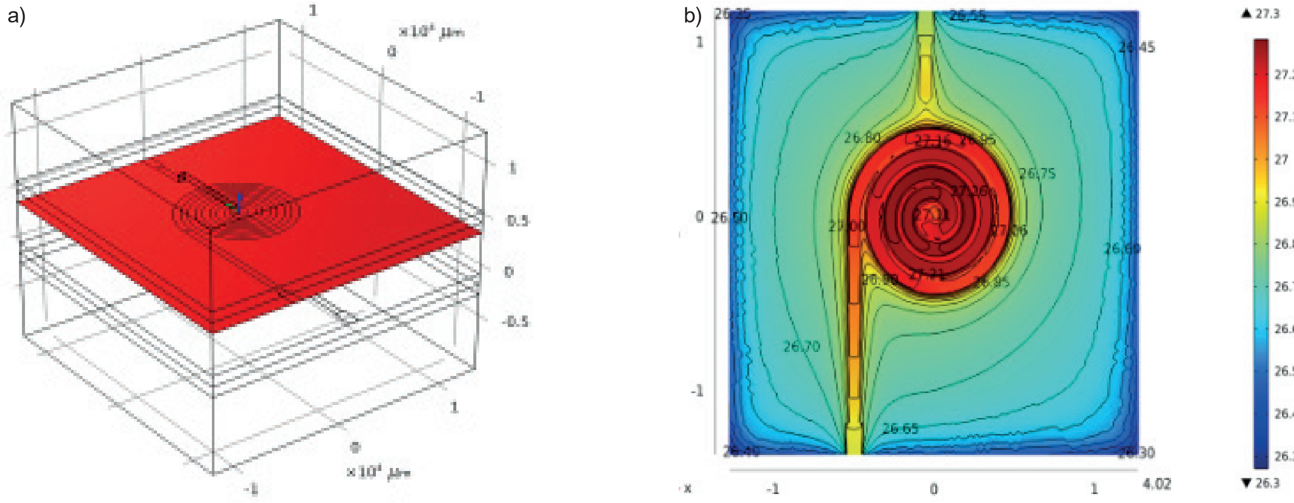

Fig. 39. (a) Horizontal plane OXY, (b) Temperature distribution in the turns of the secondary coil and isothermal curve

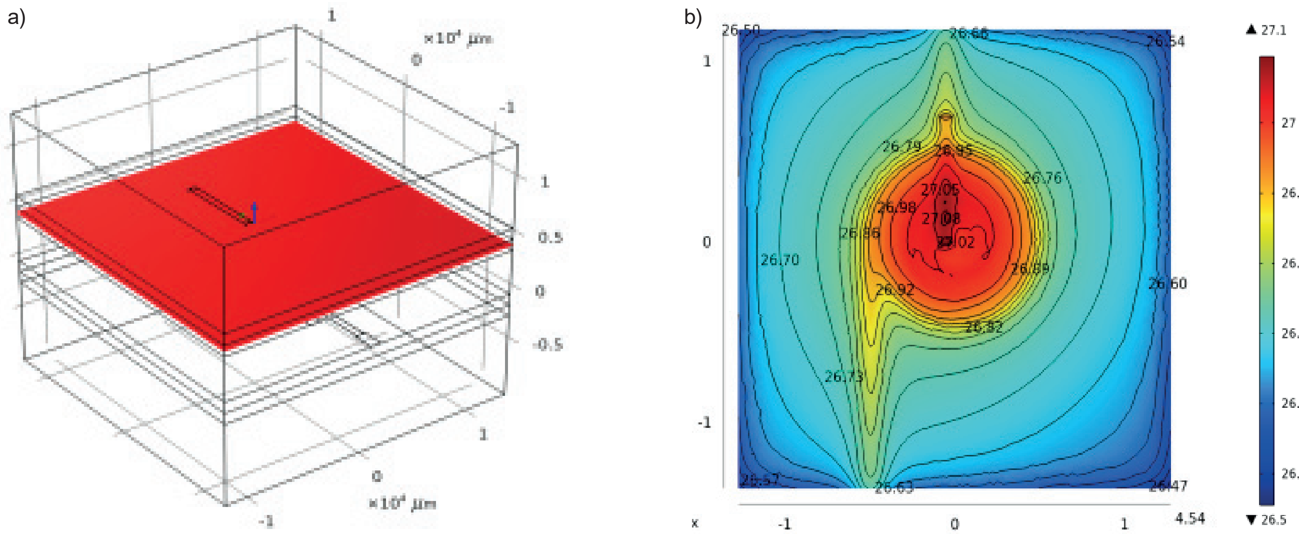

Figure.40. (a) Horizontal plane OXY, (b) Temperature distribution in the secondary Kapton medium and isothermal curve

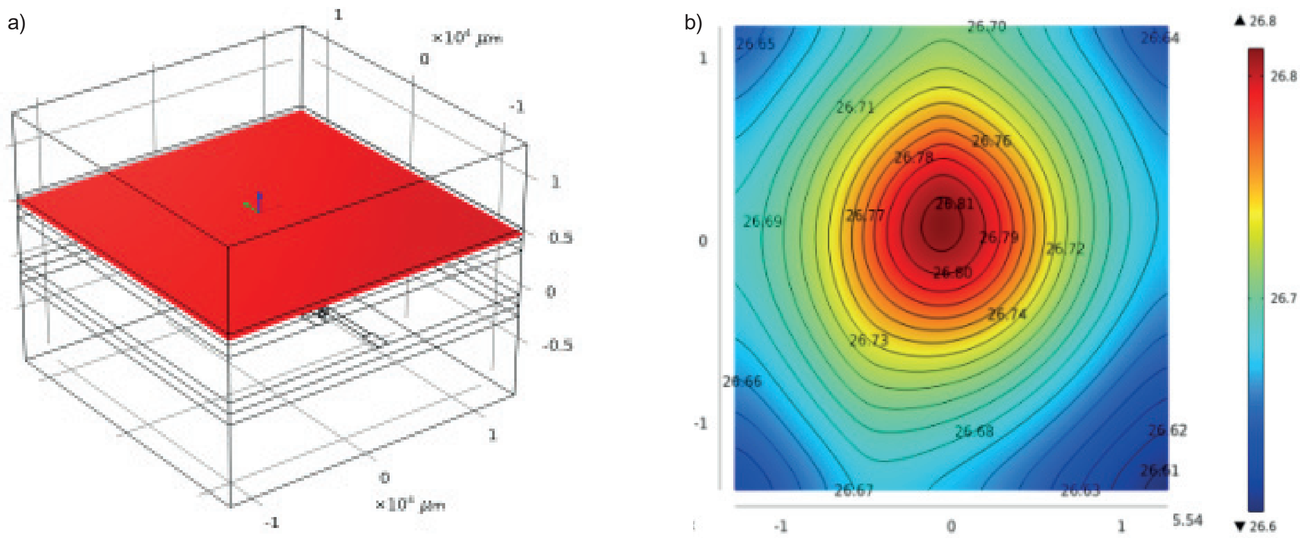

Figure.41. (a) Horizontal plane OXY, (b) Temperature distribution in the secondary NiFe2O4 medium and isothermal curve

Conclusion

The aim of this paper was to use the finite element method to model a stacked planar transformer. The study was carried out in a two- and three-dimensional frame of reference, where the unknowns are the electric potential, the current density, the magnetic field and the temperature. Maxwell's equations were used for the magnetic study and coupled with the heat equation for the thermal study. For the modeling part, we opted for the finite element method and the resolution was carried out using the Comsol Multiphysics 5.6 electrical and thermal software needed to solve our problem. The simulation results show that the temperature is higher in the micro-coil conductors, because they are the source of heat, especially in the primary coil. On the other hand, the heat flow is directed from the coils towards the substrates and the air, with the exception of the area between the two coils, where the flow is directed from the primary coil towards the secondary. For the electromagnetic component, analysis of the results showed that the electrical current density of the primary coil as a whole is greater than that of the secondary coil. This is consistent with the increase in temperature in the primary coil. There was an accumulation of current density at the inner turns due to the spike effect. We also found that the potential is greatest at the vias at the entrance to the primary and secondary micro-coils and that the magnetic field strength is greatest at the coils and magnetic substrate (the magnetic material reduces leakage).

Authors: *Redouane Mimouni was born in Oran, Algeria, on April, 21,1985. Doctoral student at University of Sciences and Technology of Oran, Algeria. Faculty of Electrical Engineering, Oran Electrical Engineering and Product Manager for Electricity at Normec BTV, Belgium. His research interests include the integration of passive components in power electronics and integrated micro-transformers. E-mail: Redouaneusto2006@hotmail.com.*
Azzedine Hamid born in Algiers, Algeria, is a professor at the El Bayadh Technology Department, Faculty of Sciences, Nour BAchir El Bayadh University Center, Algeria. He obtained his doctorate from the University of Science and Technology of Oran in 2004. His field of specialization is materials in electrical engineering and the integration of passive components. E-mail: hamidazdean@yahoo.fr
Aicha Flitti was born in Algiers, Algeria, PhD at University of Sciences and Technology of Oran, Algeria. Faculty of Electrical Engineering, Oran. His scientific interests include streamers and electric discharges. E-mail: afaouicha90@gmail.com
Abderrahim Mokhefi was born in 1992 in Oran, Algeria. He currently serves as a B-Senior Lecturer at the National Polytechnic School of Oran (ENPO). He earned his Ph.D. in energetic mechanics in 2022 from the University of Bechar (UTMB). His research interests span a variety of fields, with a primary focus on computational fluid dynamics (CFD), heat transfer, field theory, magnetohydrodynamics and nanofluids. E-mail: abderahimmokhefi@yahoo.fr
Fatima Zohra Medjaoui is currently Professor of electrical engineering anda lecturer at the University of Science and Technology of Oran city, Algeria. His research focuses on the integration of passive components in low-power electronic devices. E-mail: medjaouifaz@yahoo.fr
Mohamed Rizouga is currently Professor of electrical engineering and a lecturer at the University of Science and Technology of Oran city, Algeria. His research focuses on the integration of passive components in low-power electronic devices and electrical networks.
Authors: Redouane Mimouni, University of Sciences and Technology of Oran, Algeria; Azzedine. Hamid, University of Sciences and Technology of Oran, Algeria; Nour Bachir University Center, El Bayadh, Algérie; Aicha Flitti, Abderrahim Mokhefi, National Polytechnic School of Oran; Algeria; Fatima Zohra Medjaoui, University of Sciences and Technology of Oran, Algeria; Mohamed Rizouga

REFERENCES

[1] R. Melati, A. Hamid, L. Thierry, et M. Derkaoui, « Design of a new electrical model of a ferromagnetic planar inductor for its integration in a micro-converter », Math. Comput. Model., vol. 57, no 1, p. 200-227, janv. 2013, doi: 10.1016/j.mcm.2011.06.014.
[2] N. M. Nguyen et R. G. Meyer, « Si IC-compatible inductors and LC passive filters », IEEE J. Solid-State Circuits, vol. 25, no 4, p. 1028-1031, août 1990, doi: 10.1109/4.58301.
[3] E. Haddad, Christian Martin, Charles Joubert, Bruno Allard, Maher Soueidan, et al.., “Modeling, Fabrication, and Characterization of Planar Inductors on YIGSubstrates”, Advanced Materials Research, Trans Tech Publications, 2011, 324, pp.294–297.
[4] H. M. Greenhouse, “Design of planar rectangular microelectronic inductors”, Trans. Parts, hybrids, packaging, vol. PHP-10, n°2, pp. 101–109, Juin 1974.
[5] C. A. Chang, S.-P. Tseng, J. Y. Chuang, S.-S. Jiang, et J. A. Yeh, « Characterization of spiral inductors with patterned floating structures », IEEE Trans. Microw. Theory Tech., vol. 52, no 5, p. 1375-1381, mai 2004, DOI: 10.1109/TMTT.2004.827002
[6] S. Coulibaly, D. Malec, V. Bley, D. Mary, et B. Schlegel, « New Use of Mn-Zn Ferrite Material in Power Electronics Integrated LC Filters », Engineering, vol. 09, no 12, p. 993-1007, 2017, doi: 10.4236/eng.2017.912059.
[7] C. Wu, C.-C. Tang, et S. Liu, « Analysis of On-Chip Spiral Inductors Using the Distributed Capacitance Model », IEEE J Solid-State Circuits, vol. 38, p. 1040-1044, 2002.
[8] M. R. Benzidane, et al, “Miniaturization and Optimization of a DC–DC Boost Converter for Photovoltaic Application by Designing an Integrated Dual-Layer Inductor Model, ” Transactions on Electrical and Electronic Materials, vol. 23, p 462–475, 2022.
[9] Fred C. Lee and J. D. van Wyk “IPEM-Based Power Electronics System Integration”, Journal of Electrical Engineering www.jee.ro 94 PRZEGLĄD ELEKTROTECHNICZNY, ISSN 0033–2097, R. 94 NR 8/2018
[10] Kahina Benamer, Azzedine Hamid, Eugenia Rossi di Schio, Abderrahim Mokhefi, Rabia Melati and Paolo Valdiserri “Magnetic and Thermal Behavior of a Planar Toroidal Transformer” Energies, 2024, 17, 2454.https://doi.org/10.3390/en17112454, 21 May 2024
[11] M. R. Benzidane, et al, “Miniaturization and Optimization of a DC–DC Boost Converter for Photovoltaic Application by Designing an Integrated Dual-Layer Inductor Model, ” Transactions on Electrical and Electronic Materials, vol. 23, p 462–475, 2022.
[12] Raghavendra, Kummara Venkat Guru, et al. “A comprehensive review of DC–DC converter topologies and modulation strategies with recent advances in solar photovoltaic systems.” Electronics 9.1 (2020): 31.
[13] Melati R, Hamid A, Lebey T, Derkaoui M (2013) “Design of a new electrical model of a ferromagnetic planar inductor for its integration in a micro converter”. Math Comput Model 57:200–227
[14] Abdelkader ABDELDJEBBAR, Azzedine HAMID, Yacine GUETTAF, Rabia MELATI, “ Design of Micro-Transformer in Monolithic Technology for High Frequencies Fly-back Type Converters. Czasopismo |PRZEGLĄD LEKTROTECHNICZNY |Rocznik 2018 – zeszyt 8”
[15] M. Derkaoui, A. Hamid, T. Lebey, and R. Melati, “Design and modeling of an integrated micro-transformer in a flyback converter”. Telkomnika, vol. 11, no. 4, pp. 669–682, 2013.
[16] Rossi di Schio, Eugenia; Lazzari, Stefano; Abbati, Alessia, Natural convection effects in the heat transfer from a buried pipeline, «APPLIED THERMAL ENGINEERING», 2016, 102, pp. 227 – 233 [Scientific article]
[17] A. Allaoui, A.Hamid, P.Spiteri, V.Bley, T. Lebey “Thermal Modeling of an Integrated Inductor in a Micro-Converter” Journal of Low Power Electronics Vol 11, N^0 1 pp 63–73 (2015)
[18] Mokhefi A.; Rossi di Schio E., “Effect of a magnetic field on the couette forced convection of a buongiorno's nanofluid over an embedded cavity”, «JP JOURNAL OF HEAT AND MASS TRANSFER», 2022, 30, Article number: 14648, pp. 89 – 104